Evaluation of blood-brain barrier penetration and examination of binding to human serum albumin of 7-*O*-arylpiperazinylcoumarins as potential antipsychotic agents

Teresa Żołek[a,*], Orsolya Dömötör[b], Kinga Ostrowska[a], Éva A. Enyedy[b], Dorota Maciejewska[a,*]

[a] Department of Organic Chemistry, Faculty of Pharmacy, Medical University of Warsaw, Banacha 1, 02-097 Warsaw, Poland
[b] Department of Inorganic and Analytical Chemistry, University of Szeged, Dóm tér 7, H-6720 Szeged, Hungary

ARTICLE INFO

ABSTRACT

The delivery of drugs to the brain is complicated by the multiple factors including low blood–brain barrier (BBB) passive permeability, active BBB efflux systems, and plasma protein binding. Thus, a detailed understanding of the transport of the new potent substances through the membranes is vitally important and their physico-chemical characteristics should be analyzed at first. This work presents an evaluation of drug likeness of eight 7-*O*-arylpiperazinylcoumarin derivatives with high affinity towards serotoninergic receptors 5-HT$_{1A}$ and 5-HT$_{2A}$ with particular analysis of the requirements for the CNS chemotherapeutics. The binding constants to human serum albumin (HSA) were determined at physiological pH using fluorescence spectroscopy, and then their mode of action was explained by analysis of theoretical HSA complexes. Dynamic simulation of systems allowed for reliable evaluation of the interaction strength. The analyzed coumarins were able to pass BBB, and they present good drug likeness properties. They showed high affinities to HSA (log K_Q = 5.3–6.0 which corresponds to -8.12 to -7.15 kcalmol^{-1} of Gibbs free energy). The changes of the emission intensity upon binding to HSA were scrutinized showing the different mode of action for 4-phenylpiperazinylcoumarins. The values of computed Gibbs free energy and determined on the basis of experimentally obtained binding constants log K_Q coincide suggesting a good quality of the theoretical model. Overall the 8-acetyl-7-*O*-arylpiperazinyl-4-methyl-coumarin derivatives represent valuable lead compounds to be further tested in various preclinical assays as a possible chemotherapeutics against CNS diseases. Studied coumarins can be metabolized by cytochrome P450 to aldehydes and hydroxy derivatives. The existence of other binding sites inside HSA than Sudlow's site 1 was postulated. The longer aliphatic linker between coumarin and piperazine moieties favored binding to HSA in other than Sudlow site 1 pocket.

1. Introduction

The main challenge during the development of new medicinal substances which target the central nervous system (CNS) is to ensure that the substance is present at the pharmacological target site at sufficient concentration in order to demonstrate clinical efficacy [1]. Although the strong binding of a drug molecule to its intended target is crucial for the strength of action, poor membrane permeability could result in a lack of *in vivo* efficacy. Thus, a detailed understanding of the transport of the substance through the membranes is vitally important for pharmacokinetic analysis and for a successful drug development. Drugs that specifically target the CNS must pass three major central barriers: the blood–brain barrier (BBB) formed by capillary endothelial cells, the blood-cerebrospinal fluid barrier (CSFB) formed by choroid plexus epithelia, and the third barrier formed by tightly connected arachnoid epithelium. The absence of the intercellular pores in the
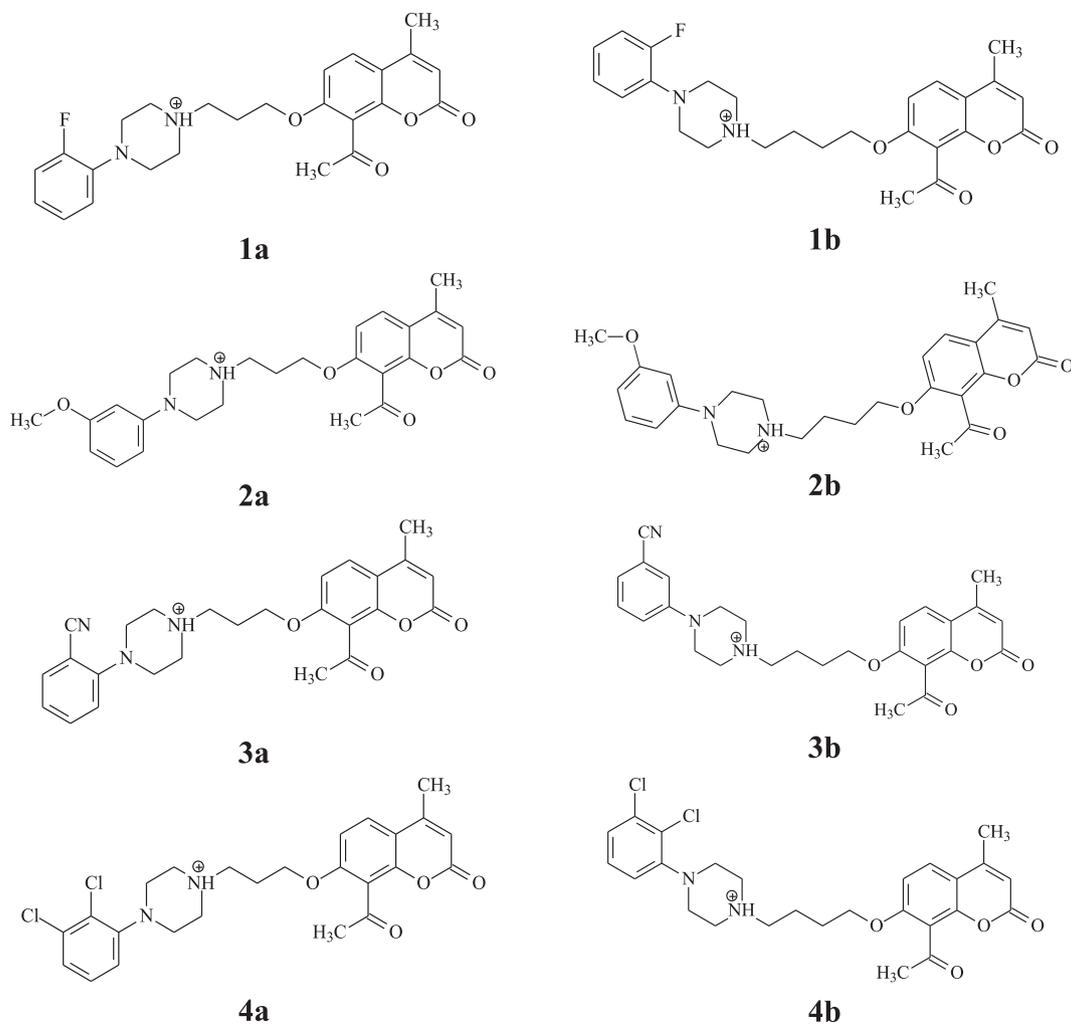
Fig. 1. The chemical structure of tested coumarin derivatives **1a–4a** and **1b–4b**.

endothelial barrier in the brain means that molecules gain access to brain interstitial fluid by the lipid-mediated free diffusion or the carrier – or receptor-mediated transport. The BBB is the most important barrier in the brain [2], that separates the brain from the rest of the body extracellular fluids and thereby protects it from potentially toxic substances in the bloodstream, as well as enables the cerebrospinal fluid of the brain to be precisely controlled [3]. Drug distribution into the cerebrospinal fluid (CSF) cannot be an indicator of BBB transport. CSF is in rapid equilibrium with the blood by convection, and the substances injected into the CSF diffuse quickly to blood, and poorly to the brain. The BBB function is enhanced by the high level of efflux transporters especially P-glycoprotein (P-gp). Strong junctions of ions and small hydrophilic molecules to P-gp reduce permeation of such solutes [4], closing any paracellular pathway [5]. Consequently, the brain-to-blood efflux systems, plasma protein binding, enzymatic activity, and cerebral blood flow can greatly alter the amount of the substance crossing the BBB. Only unionized, lipophilic and low molecular weight compounds can diffuse freely through the endothelial membrane and may passively cross the BBB if they do not bind to the efflux transporters located in the brain capillaries of endothelial cells. Small ions and polar molecules cannot cross this barrier [6,7].

Many coumarins and their derivatives underwent extensive investigations aimed to assess their beneficial effects on human health [8–10]. It has been shown, that they impact the CNS based on dopaminergic and serotonergic affinities, interactions with benzodiazepine receptors, and/or inhibition of cholinesterase and monoamine oxidases [11]. Among different pharmacological properties, their strong binding

with the CNS receptors appears to be a very important biochemical feature, and thus coumarins can be a valuable resource of chemotherapeutics for the treatment of CNS diseases. Many scientific groups search for the new antipsychotic drugs among coumarin derivatives, based on their affinities to serotonergic receptors 5-HT$_{1A}$ and 5-HT$_{2A}$ [12–14]. It was found that activities of coumarin analogs can be modulated *via* their molecular architecture. For example, it was shown that the presence of bulky aliphatic chain like a *sec*-butyl group at C-8 position decreased the antipsychotic activity, but the substitution of the methoxy group at C-3 position is favorable for their pharmacologic potential [15]. It was also observed that compounds with the *N*-arylpiperazine fragment and the methyl groups at C-3 and/or C-4 positions of the coumarin ring were the most promising ones in various biological tests [13].

Human serum albumin (HSA), one of the main carrier proteins plays an important role in the transport and disposition of exogenous and endogenous compounds present in the blood [16]. It is known that distribution in the body and pharmacological effect of chemotherapeutics are both correlated with the nature and magnitude of drug-HSA interactions. Although bound and unbound drug concentrations are predominantly in equilibrium, problems might occur if the HSA affinity of a drug is extremely high. Weak plasma protein binding leads to a short lifetime and/or poor tissue distribution of the drug and other organic compounds, whereas strong binding decreases the concentrations of free drugs in plasma [17]. The specific physiological activity of the aromatic and heterocyclic ligands upon adduct formation with serum albumin originates from the presence of two hydrophobic

pockets in subdomains IIA (Sudlow site 1) and IIIA (Sudlow site 2) of HSA [18]. HSA contains a single intrinsic tryptophan residue at position 214 in domain IIA, where a large hydrophobic cavity is present, and its fluorescence is sensitive to the ligands bound nearby [19]. Therefore, information about the HSA-ligand binding can be obtained by the measurement of intrinsic fluorescence intensity of the tryptophan residue before and after the addition of the tested compounds. HSA is a well-known transport peptide of numerous coumarin derivatives, especially for warfarin – an anticoagulant drug [20–23]. It has been reported that compounds with coumarin, chromone and chromanol rings can bind to HSA in subdomain IIA. Elimination of the 4-hydroxy group decreased the binding affinity in this series of compounds, and pyranone in not a ligand to HSA [24]. It was also shown that the acetyl group at C-8 position significantly decreased HSA binding but its role in the ligand-protein interactions was not explained definitely [25]. Therefore, additional information concerning the structural features which favor HSA binding for very potent substances evaluated *in vitro* assays is of high demand in the course of drug search. The analysis of potential drug binding to plasma protein is interesting because the unbound drug fraction affects many pharmacokinetic parameters as the steady-state distribution volume, but also it provides useful information for the design of the administration regimen dose.

In the present study, we selected eight compounds (**1a–4a**, **1b–4b**) synthesized in our research group which belongs to the 8-acetyl-7-hydroxy-4-methylcoumarin family connected with the *N*-arylpiperazine substituent *via* propyloxy or butyloxy linkers (Fig. 1). These coumarin derivatives showed very high affinities to 5-HT$_{1A}$ by *in vitro* assays (IC$_{50}$ within range 0.8–2.2 nM) and high affinities to 5-HT$_{2A}$ (8–138 nM) receptors [26], which are the initial factors in the selection of compounds to the next step in the pipeline of drug discovery which targets CNS. Before *in vivo* tests, the most favorable strategy is to calculate the most important drug likeness parameters, with special emphasis on the requirements of the CNS drugs. As a result, we evaluated ADME parameters based on the chemical structures for our set of derivatives to estimate their propensies cross BBB, as well as evaluating their toxicities. The interaction between coumarin derivatives and HSA was measured during blood transportation process *in vitro* under physiological conditions by fluorescence spectroscopy and was simulated by molecular docking and molecular dynamics (MD) methodology. We believe that this study provides basic data for clarifying the *in vivo* binding mechanisms of coumarin derivatives with human serum albumin.

2. Materials and methods

2.1. Theoretical methodology

2.1.1. Chemical structures of tested coumarins and HSA

Eight compounds were selected and studied (Fig. 1): **1a** (8-acetyl-7-{3-[4-(2-fluorophenyl)piperazin-1-yl]propoxy}-4-methylchromen-2-one), **2a** (8-acetyl-7-{3-[4-(3-methoxyphenyl)piperazin-1-yl]propoxy}-4-methylchromen-2-one), **3a** (8-acetyl-7-{3-[4-(2-cyanophenyl)piperazin-1-yl]propoxy}-4-methylchromen-2-one), **4a** (8-acetyl-7-{3-[4-(2,3-dichlorophenyl)piperazin-1-yl]propoxy}-4-methylchromen-2-one), **1b** (8-acetyl-7-{4-[4-(2-fluorophenyl)piperazin-1-yl]butoxy}-4-methylchromen-2-one), **2b** (8-acetyl-7-{4-[4-(3-methoxyphenyl)piperazin-1-yl]butoxy}-4-methylchromen-2-one), **3b** (8-acetyl-7-{4-[4-(2-cyanophenyl)piperazin-1-yl]butoxy}-4-methylchromen-2-one), and **4b** (8-acetyl-7-{4-[4-(2,3-dichlorophenyl)piperazin-1-yl]butoxy}-4-methylchromen-2-one). They belong to two groups of coumarin derivatives, which differ in the length of the linker between two rings: the coumarin and the piperidine. Namely, compounds **1a–4a** are composed with propylene but compounds **1b–4b** with a butylene linker. Coumarin derivatives are poorly soluble in water so prior biological tests they were transformed into hydrochlorides to increase their solubility. In each case, the cations were used in the theoretical studies, and the site

of protonation was proposed. The starting structures of the coumarin derivatives were constructed by Discovery Studio 2017R2 visual interface BIOVIA [27]. The geometries of all compounds were optimized using the density functional theory (DFT) with the B3LYP/6-311G (d,p) hybrid functional as implemented in Gaussian 09 [28]. The known crystal structure of HSA (PDB ID: 2BXD), which included a warfarin ligand in active site was obtained from the RCSB Protein Data Bank. Ligand, water molecules, and inorganic ions were removed, hydrogen atoms were added, and the calculations were made at the physiological pH.

2.1.2. Prediction of ADMET descriptors

ADMET parameters were computed by applying ADMET Predictor^{TM} version 8.5 program [29] using qualitative and quantitative models. Various drug likeness parameters like Lipinski's rule of five, the topological polar surface area (TPSA), the proton dissociation constants (pK_a), a Maximum Recommended Therapeutic Dose (MRTD), qualitative likelihood of penetrating the blood-brain barrier (BBB_filter) express as high/low, the logarithm of the blood-brain barrier partition coefficient logC$_{brain}$/C$_{blood}$ (logBB), percentage of unbound drug to proteins within blood plasma (%Unbnd), blood-to-plasma concentration ratio (RBP = C$_{whole-blood}$/C$_{plasma}$) and likelihood of the P-glycoprotein (P-gp) inhibition were estimated for all compounds at pH 7.4. Prediction of metabolic phase I indicators was made using cytochrome P450 (CYP 450) forms CYP 1A2, 2C9, 2C19, 2D6 and 3A4. All the CYP-metabolites generated for each compound were evaluated for risk potential whenever it was possible. Phase II metabolism of coumarin derivatives was investigated to determine the probability of whether human uridine 5′-diphosphate-glucuronosyltransferases (UGT) can be involved. Hepatotoxicity parameters were specifically studied using relevant biomarkers: alkaline phosphatase (AlkPhos), serum glutamate oxaloacetate transaminase (SGOT/AST), serum glutamate pyruvate transaminase (SGPT/ALT), γ-glutamyl transferase (GGT) and lactate dehydrogenase (LDH).

2.1.3. Starting structures of ligands by molecular docking simulations

The molecular docking experiments were carried out using the Lamarckian Genetic Algorithm (LGA) implemented in the AutoDock 4.2.3 program [30]. HSA was held rigid, all torsion bonds of the ligands were considered as free, and there was no consideration regarding the effect of solvent on the interactions. The protein input files were prepared for docking by adding Gasteiger charges on atoms. Based on the site-specific markers used in our experiment, the coumarins were docked to the Sudlow site 1. The size of the grid box was defined in the shape of a three-dimensional grid (50 × 50 × 50 Å) at a resolution of 0.375 Å. The docking parameters used were as follows: GA population size: 150 and the maximum number of energy evaluations: 250 000. During docking, a maximum number of top 30 conformers was considered, and the root means square (RMS) cluster tolerance was set to 2 Å. The conformers corresponding to the lowest free energy were used as the starting points in the MD simulations.

2.1.4. HSA-ligand complexes by molecular dynamics simulations

MD simulations of the ligand-HSA complexes were performed in solution to better reflect experimental systems and the intermolecular interactions which play a crucial role in their stability. We used the CHARMm force field [31] implemented in the module of Discovery Studio 2017R2. Each protein-ligand complex was immersed in a cubic box of TIP3P water molecules [32] (12 Å from the solute surface) and neutralized by the addition of chloride anions. The MD strategy consisted of two-step energy minimization of the solvated complexes. First of all, the water molecules were optimized using the steepest descent method with 1000 steps, and then the conjugate gradient method was employed for another 1000 steps while protein and ligand were kept frozen. The restraints were weak with force constant of 10 kcal mol^{-1} Å^{-2}. Secondly, using the same approach in the first step above was

performed with all atoms relaxed. The MD protocol contained a heating step performed for 50 ps up to 300 K. Before proceeding to production, MD step equilibration was done at 300 K for 50 ps. In the stages of heating and equilibration, the solutes (protein and ligand) were fixed with force constant of $2 \, kcal \, mol^{-1} \, Å^{-2}$. The equilibrated system was taken as the starting structure for production runs using two phases. In the first phase, NVT was performed at 300 K for 200 ps in the presence of a weak harmonic restraint on the solute, and in the second phase NPT at 300 K and 1 bar for 5 ns. The periodic boundary conditions were used and the motion equations were integrated by applying the Leapfrog Verlet algorithm [33] with a time step of 2 fs. The trajectories were recorded at 10 ps interval.

2.1.5. Binding free enthalpy calculations using MM-PBSA

The free enthalpy calculations were carried out using the MM-PBSA approach [34] embedded in Discovery Studio 2017R2. The atomic coordinates of HSA and each ligand were extracted from a single trajectory of the MD simulations obtained using explicit water molecules. Each binding free enthalpy was calculated based on the average structures obtained from the last 2 ns of MD trajectories. The components of each complex were minimized using the conjugate gradient method for 10 000 steps after 100 steps of the steepest descent algorithm and a dielectric constant of 4 for the electrostatic interactions until the RMS gradient of the structure was less than $0.001 \, kcal \, mol^{-1} \, Å^{-1}$. The binding free enthalpy (ΔG_{bind}) between a ligand and a protein was estimated given the functional form of MM-PBSA formalism in Eq. (1).

$$\Delta G_{bind} = G_{HSA-ligand} - (G_{HSA} + G_{ligand}) \qquad (1)$$

where $G_{HSA\text{-}ligand}$ is free enthalpy of complex, G_{HSA} is free enthalpy of HSA and G_{ligand} is free enthalpy coumarin derivative.

2.2. Experimental methodology

The lipophilicities and the dissociation constants for coumarin derivatives together with equilibrium constants for HSA-ligand complexes were determined experimentally.

2.2.1. Preparation of stock solutions of HSA and coumarins

HSA (with fatty acids as lyophilized powder), KOH, HCl, KCl and all buffer components used for lipophilicity measurements are Sigma-Aldrich products in *puriss* quality. Milli-Q ultrapure water was used as a solvent of the samples and stock solutions. HSA solution was prepared in phosphate buffer (20 mM, pH 7.40) containing 0.1 M KCl strictly on the same day as the experiment was done. Estimated concentration of HSA stock solutions was calculated from its UV absorption: $\varepsilon_{280 \, nm}(HSA) = 36850 \, M^{-1} \, cm^{-1}$ [35]. Hydrochloride salts of the coumarin derivatives were dissolved in slightly acidic water (pH ~ 4) at 100 μM concentration.

2.2.2. Estimation of pH-dependent lipophilicity and proton dissociation constants (pK_a) for coumarins

Distribution coefficient (D_{pH}) values of the compounds were determined by the traditional shake-flask method in *n*-octanol/buffered aqueous solution at various pH values at 25.0 ± 0.2 °C. pH values of the samples were adjusted with *n*-octanol pre-saturated aqueous solutions containing different buffer systems at *ca.* 50 mM concentration and 0.10 M KCl. Applied pH values are follows: pH 2.01 (H_3PO_4/NaH_2PO_4); pH 3.01 (formic acid/Na-formate); pH 4.01 (formic acid/Na-formate); pH 5.01 (acetic acid/Na-acetate); pH 5.41 (2-(*N*-morpholino)ethanesulfonic acid (MES)/its Na-salt); pH 6.03 (MES/its Na-salt); pH 6.53 (MES/its Na-salt); pH 7.04 (NaH_2PO_4/Na_2HPO_4); pH 7.50 (NaH_2PO_4/Na_2HPO_4); pH 8.45 (NH_4Cl/NH_3); pH 8.97 (NH_4Cl/NH_3); pH 10.30 (3-(cyclohexylamino)-1-propanesulfonic acid (CAPS)/its Na salt). Compounds were dissolved in slightly acidic *n*-octanol pre-saturated water (pH ~ 4, I = 0.10 M KCl) and aliquots were mixed with

the certain buffer systems in 1:2 vol ratio in order to get the stock solutions. Final compound concentration was 5–40 μM, and exact pH values were measured with an Orion 710A pH-meter equipped with a Metrohm combined electrode (type 6.0234.100) after three-point calibration of the electrode system. Stock solutions and water presaturated *n*-octanol were gently mixed in 1:1, 1:0.02 or 1:0.01 vol ratio with Heidolph Reax 2 overhead shaker (~ 20 revolutions per minute (rpm)) for 2 h. The mixtures were centrifuged with Eppendorf MiniSpin Plus centrifuge (5000 rpm, 3 min). After phase separation, UV−visible (UV−vis) spectrum of the compound in the aqueous phase was compared to that of the original stock solutions and D_{pH} values of the compounds were calculated according to the following equation (Eq. (2)):

$$D_{pH} = \left[\frac{Abs_{(stock. \, sol.)}}{Abs_{(aqueous \, phase \, after \, separation)}} - 1 \right] \times \frac{V_{(aqueous \, phase)}}{V_{(n\text{-}octanol)}} \qquad (2)$$

A Thermo Scientific Evolution spectrophotometer and a Hewlett Packard 8452A diode array spectrophotometer were used to measure the UV–vis spectra in the interval 200–500 nm.

pH dependence of the D_{pH} values were utilized to estimate proton dissociation constants (pK_a) of **1a–4a** and **1b–4b**. According to our model both protonated (HL^+) and charge neutral (L) species distribute between the polar and non-polar solvent phases, namely both P_{HL^+} and P_L constants can be derived from the measurements since D_{pH} value is equal to the corresponding partition coefficient (P) value in that pH range where the compound is presented practically in one single protonation state (either HL^+ or L). The pK_a values were calculated according to Eq. (3):

$$K_a = \frac{(P_{HL^+} - D_{pH}) \times [H^+]}{(D_{pH} - P_L)} \qquad (3)$$

where $[H^+]$ is the free proton concentration in aqueous phase calculated from the measured pH. The pK_a values were fitted with the computer program PSEQUAD [36] using the pH − D_{pH} data pairs and P_{HL^+}, P_L constants. A more detailed description of lipophilicity models and model selection can be found in the Supplementary Materials.

2.2.3. Spectrofluorometric measurements of interaction with HSA

Phosphate buffer (20 mM, pH 7.4) with 0.10 M KCl was used for sample preparation; spectra were recorded after 10 min incubation. Two kinds of experiments were carried out: 1 μM HSA and various amounts of coumarin compound (from 0 to 25 eq.) were used for quenching experiments; and intrinsic fluorescence of the compounds was examined in samples containing 2.4–3.3 μM compound and 0–23 μM HSA. The excitation wavelength was chosen for 295 nm in quenching experiments; the emission intensities were read in the range of 310–500 nm with 5 nm/5 nm slit widths. In the second experiment, compounds were excited at 330 nm; the emission was recorded in the range of 340–550 nm with slit widths of 10 nm/10 nm. Spectra were corrected by the light scattering effect of HSA appearing at these conditions. Computer program PSEQUAD was utilized for calculation of equilibrium constants for HSA−ligand complexes from both types of experiments as described in our former work [37].
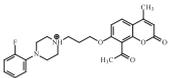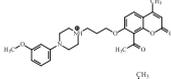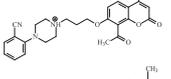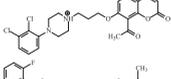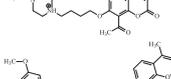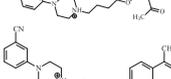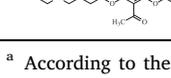
Three-dimensional fluorescence spectra were obtained between 230 and 400 nm excitation and 250–550 nm emission wavelengths with slit widths of 5 nm/5 nm. Corrections for self-absorbance and inner filter effect were necessary since the exciting and emitted light were partly absorbed by the compounds. The following formula (Eq. (4)) was used for spectral correction:

$$F_{corrected} = F_{measured} \times 10^{\frac{(A_{(EX)} + A_{(EM)})}{2}} \qquad (4)$$

where corrected fluorescence ($F_{corrected}$) is given as the product of the measured intensity ($F_{measured}$) and 10 to the power of average absorbances measured at the excitation ($A_{(EX)}$) and emission wavelengths ($A_{(EM)}$).

Table 1
Theoretical values of topological polar surface area (TPSA), percentage of unbound drug to blood plasma proteins (%Unbnd), blood-to-plasma concentration ratio (RBP), BBB filter, blood-brain barrier partition coefficient (logBB), likelihood of the P-glycoprotein inhibition (P-gp) and predicted proton dissociation constants (pK_a) for coumarins **1a–4a** and **1b–4b**.

Compound		TPSA Expected values	%Unbnd	RBP	BBB filter	logBB[a]	P-gp	pK_a
		(≤ 90 Å^2)	(> 10%)	(< 1)	(High/low)			
	1a	62.99	1.771	0.655	High	0.183	I	6.98
	2a	72.22	1.937	0.627	High	−0.190	I	6.74
	3a	86.78	2.301	0.608	High	−0.610	I	6.93
	4a	62.99	0.865	0.667	High	0.257	I	6.99
	1b	62.99	2.065	0.648	High	0.282	I	7.39
	2b	72.22	2.099	0.622	High	−0.096	I	7.20
	3b	86.78	2.347	0.604	High	−0.543	I	7.14
	4b	62.99	0.997	0.660	High	0.368	I	7.41

[a] According to the classification made by Ma et al. [57]: high absorption to CNS: logBB more than 0.3; middle absorption to CNS: logBB 0.3 – (−1.0); low absorption to CNS: logBB less than −1.0.

3. Results and discussion

3.1. Assessing of ADMET parameters

3.1.1. Blood-brain barrier in silico assay

The physico-chemical parameters with relation to Lipiński's rule of five are presented in the Supplementary Material, Table S1 for **1a–4a** and **1b–4b**. As can be seen, the tested coumarins fulfill the majority of basic requirements for orally administrated drugs. Only the values of molecular weight (MWt) and log D are fairly high for **4b** with the two chlorine substituents. Since these parameters should be in specific range for substances aimed at the CNS their values were scrutinized below together with the following parameters being crucial for evaluation of BBB penetration which are shown in Table 1. The topological polar surface area (TPSA) is a key parameter for prediction of CNS penetration. TPSA was suggested to be a measure of a molecule's hydrogen bonding and its value should not exceed certain limit lower than for other drug's classes [38,39]. Two limits were proposed, namely a lower limit of 60–70 Å^2 and a higher limit of 90 Å^2 [40–42]. TPSA values of all compounds in our study are in these ranges which creates basic conditions for the penetration BBB. MWt is an important parameter determining the lipid-mediated free diffusion of molecules across the BBB. Small molecules may cross the BBB due to their MWt lower than 400–500 g mol^{-1}, however, according to the suggestion of van de Waterbeemd et al. [43], MWt should be below 450 g mol^{-1} or even below 400 g mol^{-1} [44], because the BBB is a specialized structure between the cerebral capillaries and the brain parenchyma. Only **1a** and **3a**, reported herein, have MWts ≤ 450, but **2a**, **1b** and **3b** show values close to 450 g mol^{-1}. Nevertheless, larger molecules can be transported by receptor- or transporter-mediated systems. Another important drug property that governs permeation across the CNS tissue

barrier is the molecular lipophilicity, expressed as log P, where P is the partition coefficient. Capillaries of the brain are devoid of aqueous pores which facilitate aqueous diffusion, thus lipid diffusion becomes a critical determinant of BBB drug penetration, and a higher lipophilicity is required to achieve greater CNS efficacy. On the other hand, the more lipophilic compounds frequently demonstrate a higher level of binding to serum proteins. From the other side, the lowest log P values of ∼ 2 were suggested to be the most optimal to minimize the metabolism and toxic side effects. Thus, lipophilicity and protein binding can be considered as conflicting characteristics in regard to CNS penetration. The BBB penetration was optimal for several classes of CNS active substances when log P values were in the range of 2–5 [45,46]. The log P values for tested coumarins were in the range 3.41–4.98 close to that of marketed CNS drugs. The logarithm of the distribution coefficient (log D), which characterized ionic substances, needs to be greater than 0 and less than 4 for better brain permeation [43]. For eight analyzed coumarins log D values are lower than log P values and fall within the range 3.32–4.68. Only derivatives **4a** and **4b** with two Cl substituents show relatively high log D values, which indicates a higher probability of binding to plasma proteins. An important parameter is hydrogen bonding that occurs with the surrounding medium i.e. water. It has been reported that for a compound to be transported through the BBB, the H-bond donors should be ≤ 3 and H-bond acceptors should be ≤ 7 [47]. An inspection of the investigated coumarins H-bond donors and acceptors suggests that all have a potential to effectively cross the BBB. A specific attention was given to the proton dissociation constant (pK_a). Fischer et al. [48], estimated pK_a limit between 4 and 10 in a study of comparative properties for BBB penetration. The predicted pK_a values of all compounds fall in the range of 6.74–7.41 (Table 1) and the shortening the linker from the butylene to the propylene chain decreases the pK_a values. The computed values are in good agreement

with the experimental values (see Section 3.2).

On the basis of our findings, the calculated BBB permeation parameters as BBB_filter and blood-brain barrier partition coefficient logBB are promising for tested coumarins (Table 1). BBB_filter is a qualitative likelihood of crossing the BBB and logBB is a measure of the partitioning between brain and blood tissue, quantified by the ratio of the solute concentrations in brain and blood. The BBB_filter parameter is indicated as high, and the values of logBB's are found in the range from −0.610 to 0.368, that correlates with the permeation of high-to-moderate for all tested compounds. The logBB values for three compounds **1b**, **4a** and **4b**, with halogen atoms were found to be close to 0.3 values, suggesting that this kind of substitution increases the potential of drugs for BBB penetration. Compounds **3a** and **3b** with cyano group have the lowest logBB values (close to −0.6) suggesting an unfavorable impact of cyano group on BBB crossing.

Yet another important property of a potential drug is its ability to bind to plasma proteins (HSA and α_1-acid glycoprotein (AGP)), which is in most cases considered as undesirable. Depending on the drug and the target, high affinity to plasma proteins may consequently increase or decrease the efficacy of drug transport. A drug bound weaker can more efficiently traverse cell membranes or diffuse. The active efflux transporter at the BBB is P-glycoprotein (P-gp), which performs active back-transport of drugs from the brain to blood. A successful CNS drug should not be an efficient P-gp substrate (*in vivo*) and also possess low-affinity to serum albumin ($K_D < 10\,\mu M$) [49]. Three theoretical parameters characterize these properties: the percent of drug unbound to protein within blood plasma – %Unbnd, the concentration of the drug in whole blood compared to plasma – RBP, and the mode of the interaction with P-gp. For the analyzed coumarins the values of %Unbnd are in the region 0.997–2.347%, and the values of RBP in the region 0.604–0.667 (Table 1), what suggests that all compounds fall in the region of strong plasma protein binding.
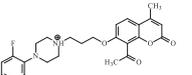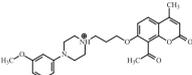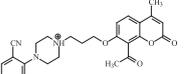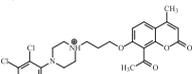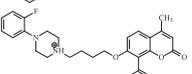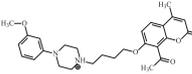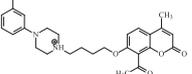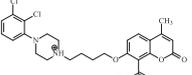
Emerging evidence has highlighted a potential role for the efflux transporter P-gp expressed at the BBB in the etiology of treatment-resistant depression [50,51]. This neurological disorder can be improved by inhibiting drug efflux at the blood–brain barrier. In our study, **1a–4a** and **1b–4b** exert P-gp inhibition effects (Table 1) what suggests that those coumarins can suppress P-gp activity and can be considered as promising compounds for further development steps as novel therapeutic agents.

3.1.2. Biotransformation of the tested coumarins

The processes of drug biotransformation are the enzymatic conversions of the drugs to their metabolites which are classified as either phase I or phase II reactions based on the nature of the chemical modifications and the enzymes involved. The majority of phase I reactions are mediated by a large family of CYP450 enzymes, while phase II occurs predominantly by the UGT enzymes, distributed in various organs in human body. Modes of action (inhibition/substrate) for different isoforms CYP450 are presented in Table 2. All studied coumarins are possible substrates for isoenzymes CYP1A2 and CYP2C19 and, on the other hand, are likely to inhibit CYP2C9. Compounds (**3a** and **3b**) with (2-cyanophenyl) piperazinyl moiety cannot be metabolized by CYP2D6 isoform, while the other tested coumarins may be substrates and inhibitors to both CYP2D6 and CYP3A4. Hypothetical metabolites of tested coumarins are presented in Fig. S1 in Supplementary Materials. We can see those main metabolites are aldehydes (up to 64%) which are formed by breaking the C−N bond at the piperazine ring. The remaining metabolites are formed by hydroxylation of the benzene ring or the methyl group at C-4 atom in coumarin ring moiety. Additionally, nine main microsomal hepatic UGTs were examined to identify which isoforms may be responsible for coumarins glucuronidation reaction leading to their easier elimination. All coumarins are predicted to be substrate for only one isoenzyme 1A4, whereas none of them was predicted to be substrate for isoenzymes 1A1, 1A3, 1A6, 1A8, 1A9, 1A10, 2B7 and 2B15 (see Table S2 in Supplementary Materials).

Table 2
Prediction of interactions with various isoforms of hepatic microsomal cytochromes CYP450 enzymes for coumarins **1a–4a** and **1b–4b**.

Compound		CYP Mode of action				
		1A2	2C9	2C19	2D6	3A4
	1a	S	I	S	I/S	I/S
	2a	S	I	S	I/S	I/S
	3a	S	I	S	I	I/S
	4a	S	I	S	I/S	I/S
	1b	S	I	S	I/S	I/S
	2b	S	I	S	I/S	I/S
	3b	S	I	S	I	I/S
	4b	S	I	S	I/S	I/S

I – denotes inhibition of CYP isoforms; S – denotes substrate for CYP isoform.
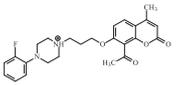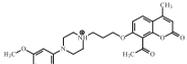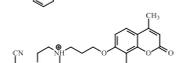
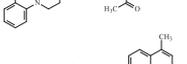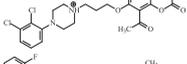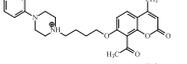### 3.1.3. Prediction of toxic effects

The predicted values of toxicity parameter for coumarins **1a–4a** and **1b–4b** are shown in Table 3. Among these toxicity parameters, MRTD represents a qualitative assessment of maximum recommended therapeutic dose administrated orally. To develop an effective oral drug, the MRTD value should be greater than 3.16 (mg/kg-bw/day), which can indicate that the selected compound has fewer side effects. Compounds **2a**, **2b**, **4a**, and **4b** have MRTD value greater than 3.16, indicating that the appearance of side effects is less likely for these compounds. Among compounds with MRTD values below 3.16 (mg/kg-bw/day) are derivatives with fluoro and cyano substituents. Further parameters are related to a liver toxicity. During a screening, all coumarin derivatives being predicted as "non-toxic" taking into account relevant biomarkers (AlkPhos, GGT, LDH, SGOT, and SGPT).

3.2. Proton dissociation equilibria and intrinsic fluorescence of the tested coumarins

All investigated compounds have a poor aqueous solubility, accordingly UV–vis spectrophotometry, that requires lower concentrations, was used for first to monitor their proton dissociation processes at highly diluted concentrations (2–20 μM) in pure aqueous solution. Molar absorbance of the studied compounds at acidic conditions (pH 2.5) ranges from $\varepsilon = 11600$ to $17100\,M^{-1}cm^{-1}$ with $\lambda_{max} = 321–322\,nm$ (see Table 4). However, these intense ligand bands were found to be fairly insensitive to the (de)protonation of the molecules. Only compound **2a** (see Fig. 2) shows the tendentious but weak spectral changes at pH between 5.0 and 8.5, and a pK_a value of 7.06 ± 0.01 could be calculated for this process. The deprotonation constant most probably belongs to one of the piperazine nitrogens, *i.e.* to the proton dissociation of the $^+NH−CH_2$ moiety. Since chromophore

Table 3
Predicted toxicity parameters for coumarins **1a–4a** and **1b–4b**: maximum recommended therapeutic dose MRTD, level of alkaline phosphatase (AlkPhos); level of γ-glutamyl transferase (GGT), level of serum glutamate oxaloacetate transaminase (SGOT), level of serum glutamate pyruvate transaminase (SGPT), level of lactate dehydrogenase (LDH).

Compound		MRDT Expected values	AlkPhos	GGT	LDH	SGOT	SGPT
		(> 3.16 mg/kg/day)					
	1a	Below 3.16	NT	NT	NT	NT	NT
	2a	Above 3.16	NT	NT	NT	NT	NT
	3a	Below 3.16	NT	NT	NT	NT	NT
	4a	Above 3.16	NT	NT	NT	NT	NT
	1b	Below 3.16	NT	NT	NT	NT	NT
	2b	Above 3.16	NT	NT	NT	NT	NT
	3b	Below 3.16	NT	NT	NT	NT	NT
	4b	Above 3.16	NT	NT	NT	NT	NT

groups (coumarin and phenyl) are situated relatively far from this piperazine nitrogen, UV absorption spectra are nearly insensitive to the (de)protonation processes.

In order to obtain information about the protonation equilibrium of the other compounds as well, pH-dependent lipophilicity studies were carried out. The strongly lipophilic nature of the studied compounds required modified experimental conditions, namely the water-to-octanol volume ratio was changed in favor of the water (see details in Section 2.2.2). Two models were considered for the calculations (see details in the Supplementary Materials, Section S-2). Fig. 3 shows the *n*-octanol/water distribution coefficients (D_{pH}) of **2a** determined at different pH values. D_{pH} values in Fig. 3 clearly reveal the distribution of the HL^+ species between the *n*-octanol and the aqueous phase, since D_{pH} values are larger than zero even at the lower pH range (when only HL^+ species is present in the solution). Measured D_{pH} values show a sigmoidal shape in dependence of the pH and the inflection point of this curve corresponds to the pK_a of compound **2a**, which was fitted with the computer program PSEQUAD using the pH – D_{pH} data pairs. In contrasts to the most widely accepted model (model 1), where an only distribution of the neutral form is expected (dashed line in Fig. 3), our

Table 4
Proton dissociation constants (pK_a) for coumarins **1a–4a** and **1b–4b** estimated from the pH-dependence of *n*-octanol/water distribution coefficient (D_{pH}) values; distribution of the ligand species at pH 7.40 in water; partition coefficients (P) of the ligand species L and HL^+ and distribution coefficient ($D_{7.4}$) at pH 7.40 in *n*-octanol/water; absorption maximum (λ_{max}) and molar absorbance (ε) of the HL^+ form; $\lambda(EM)_{max}$ and relative fluorescence emission intensity values for the compounds at pH 7.4; conditional binding constants to HSA on site 1 (log K_Q) ($t = 25 °C$, I = 0.10 M KCl).

	1a	2a	3a	4a	1b	2b	3b	4b
pK_a UV–vis	6.95 ± 0.04	6.86 ± 0.03[a]	6.90 ± 0.04	6.35 ± 0.08	7.20 ± 0.05	7.13 ± 0.04	7.15 ± 0.04	6.72[b]
$HL^+_{7.40}$ (%)	26	22	24	8	39	35	36	17[b]
$L_{7.40}$ (%)	74	78	76	92	61	65	64	83[b]
log P_L	3.26 ± 0.01	2.95 ± 0.01	3.14 ± 0.02	3.5 ± 0.1	3.41 ± 0.03	3.08 ± 0.04	3.27 ± 0.05	3.65[b]
log P_{HL+}	0.84 ± 0.08	0.84 ± 0.06	0.61 ± 0.09	1.96 ± 0.06	0.97 ± 0.08	0.90 ± 0.04	0.80 ± 0.08	–
log $D_{7.40}$	3.11	2.80	2.99	3.35	3.26	2.93	3.12	3.52[b]
λ_{max}/nm (ε/M^{-1} cm^{-1}) of HL^+	321(12400)	321(14100)	321(15500)	321(11600)	322(14100)	322(17100)	322(16700)	322(13900)
$\lambda(EM)_{max}$ (nm)	422	424	405	424	423	424	397	408
Relative intensity[c]	0.29	0.31	0.64	0.29	0.41	0.46	1.00	0.54
log K_Q (HSA)[d]	5.25 ± 0.1	5.33 ± 0.1	5.75 ± 0.1	5.96 ± 0.1	n.d	n.d.	5.70 ± 0.1	5.88 ± 0.1
K_D[e]	5.6 µM	4.7 µM	1.8 µM	1.1 µM	–	–	2.0 µM	1.3 µM

[a] pK_a = 7.06 ± 0.01 determined by UV–vis spectrophotometric titrations.
[b] Predicted value based on the tendencies of the other derivatives.
[c] Relative fluorescence intensities measured at emission maxima and at λ(EX) = 322 nm at pH 7.4.
[d] Measured at pH 7.4 (20 mM phosphate buffer, 0.1 M KCl).
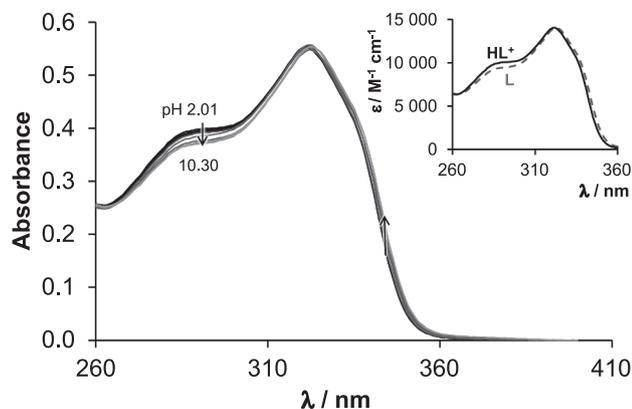[e] K_D = dissociation constant of the HSA adduct ($K_D = 1/K_Q$).

Fig. 2. pH-Dependent UV–vis spectra of **2a** and at the upper side calculated individual molar spectra of the ligand species in the two protonation states L and HL$^+$. (c = 19.6 μM; l = 2 cm; t = 25 °C; I = 0.10 M (KCl)).
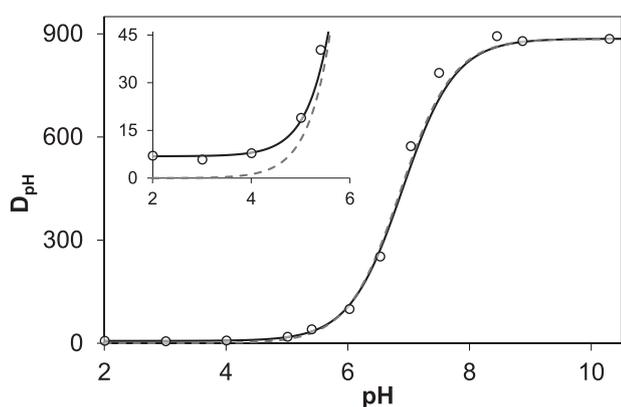

Fig. 3. Measured (○) and fitted distribution coefficients (D$_{pH}$) for **2a** at different pH values. Fitted curves correspond to the model 1 where only the distribution of the neutral form is expected (dashed line), and to the model 2 where both L and HL$^+$ forms may distribute between the polar and *non*-polar phases (solid line). The inset shows the initial part of the functions in the pH range from 2.0 to 6.0. (D$_{pH}$ values were determined in *n*-octanol/water system at the indicated pH values by traditional shake flask method; see details in the Section 2.2.2).

method operates with the partition of both protonation states (model 2). Obtained pK_a, log P$_L$ and log P$_{HL}$ values are listed in Table 4. The lipophilicity of tested coumarins is within the limits for the drugs targeted CNS. The pK_a values determined in aqueous solution are in the range of 6.35–7.20. It is clear that displacement of the propylene linker between the piperazine and coumarin moieties to butylene linker tendentiously increases the log P$_L$ and pK_a values. This phenomenon helped us to predict these constants for **4b** (see Supplementary Materials, Section S-3, Fig. S3), that was found to be fairly insoluble in water at pH > 6.5. Chloride substitution of the compounds undoubtedly results in increased acidity due to its high electronegativity. Fluorine monosubstitution interestingly leads to a small increase in the pK_a values compared to the methoxy derivatives, and nitrile substitution has only a minor effect on the acidity of the compound as well. Notably, the computed pK_a values are in good agreement with the constants reported in our former work for their structural analogues containing the same 4-(4-phenylpiperazin-1-yl)propyloxy or -butyloxy group but in a different position on the coumarin ring. Furthermore, the experimental pK_a values fit well to the predicted ones in the case of ligands **1a**, **1b**, **2a**, **2b**, **3a**, and **3b**, although they differ more significantly for the dichlorine substituted **4a** and **4b**.

Species distribution was calculated at pH 7.4 based on the determined pK_a values (Table 4). All the studied coumarins are protonated partly at this particular pH, but 61–92% are present in the neutral (L)

form. Distribution coefficients (D$_{7.40}$) calculated for pH 7.4 reflect the highly lipophilic character of the predominant neutral forms, and even HL$^+$ forms are still lipophilic according to the log P$_{HL}$ values determined. The fluorescent activity of the compounds is expected as they contain the coumarin moiety. Accordingly, their intrinsic fluorescence was examined and the position of emission maxima (λ$_{(EM)max}$) are collected in Table 4. We have found that all compounds are weakly fluorescent and the actual protonation state of the molecules has no considerable effect on it. The characteristic high emission of 3-methyl coumarins is most probably quenched by the acetyl substitution at position 8 on the coumarin ring [52]. The butoxy derivatives show somewhat higher fluorescence compared to their propoxy counterparts, **3a** and **3b** are the most emissive compounds.

3.3. Interaction with HSA: spectrofluorometric studies

The interaction of compounds **1a–4a** and **1b–4b** with human serum albumin (HSA) was investigated by fluorescence spectroscopy *via* the intrinsic fluorescence of the protein and the compounds as well. HSA, as the most abundant protein constituent of blood plasma, has outstanding capacity to transport a wide variety of endogenous compounds (e.g. fatty acids, bilirubin, steroids, and metal ions) and pharmaceutics. Its concentration in blood plasma is *ca.* 630 μM [53,54]. HSA comprises hydrophobic binding sites 1, 2 and 3 located in the hydrophobic pockets in subdomains IIA, IIIA and IB respectively. The only tryptophan (Trp214) residue in HSA is responsible for most of the intrinsic fluorescence of the protein and it is located near to site 1. Trp214 can be selectively excited at λ = 295 nm and it shows strong fluorescence between 310 and 400 nm (with a maximum at 340 nm) that can be attenuated by a binding event at or close to Trp-214 owing to its susceptibility to changes in its environment [53–55]. Thus, direct studies on the binding at the primarily assumed binding pocket become possible.

The HSA – compound interaction was revealed to be quite fast in time-dependence measurements (completed within few seconds, see Fig. S4 in Supplementary Materials), therefore 10 min incubation time was used to ensure the equilibrium state for the HSA binding experiments. A correction equation was used to reduce to significant self-absorption and inner filter effect of the compounds. Representative emission spectra are presented in Fig. 4 for the **4a** – HSA system and in the Supplementary Materials, Fig S5 for the **1b** – HSA system. As the studied compounds are fluorescent themselves, their intrinsic emission bands partly overlap with that of HSA. This phenomenon did not hinder the determination of quenching constant. The two calculation methods, namely when restricted wavelength range (310 – ca. 340 nm) was used and the emission originated from the ligand was eliminated or when all
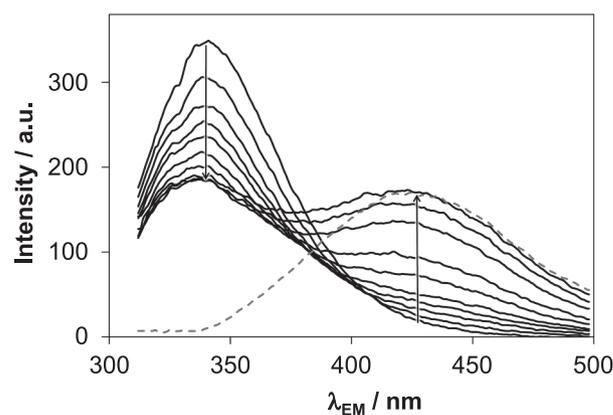

Fig. 4. Fluorescence emission spectra of HSA – **4a** system. The grey dotted line shows the spectrum for **4a** alone at 10 μM concentration. (c$_{HSA}$ = 1 μM; c$_{comp}$ = 0–10 μM; λ$_{EX}$ = 295 nm; t = 25 °C; pH 7.40 (20 mM phosphate buffer); I = 0.1 M (KCl)).

Fig. 7. Emission spectra of **3a** upon addition of HSA. Inset shows the intensity changes at $\lambda_{EM} = 410$ nm. ($c_{comp} = 2.8\,\mu M$; $c_{HSA} = 0$–$23\,\mu M$; $\lambda_{EX} = 330$ nm; $t = 25\,°C$; pH 7.40 (20 mM phosphate buffer); I = 0.10 M (KCl)). Spectra are corrected by the light scattering effect of HSA, see details in the Supplementary Materials, Fig S6.
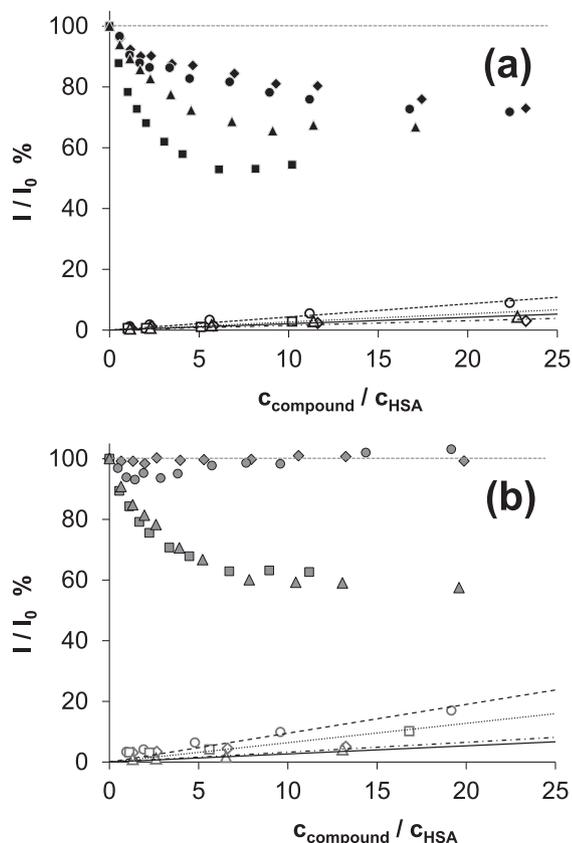
Fig. 5. Measured quenching of the Trp fluorescence emission intensity of HSA as I/I_0 (%) by the addition of the propyloxy derivatives (**a**): **1a** (♦), **2a** (●); **3a** (▲); **4a** (■), and butyloxy derivatives (**b**): **1b** (♦); **2b** (●); **3b** (▲); **4b** (■). Empty symbols correspond to the relative emission of the compounds alone. ($c_{HSA} = 1\,\mu M$; $\lambda_{EX} = 295$ nm; $\lambda_{EM} = 340$ nm; $t = 25\,°C$; pH 7.40 (20 mM phosphate buffer); I = 0.10 M (KCl)).

the three components (HSA, HSA – ligand and unbound ligand) were considered to be fluorescent provided similar quenching constants (log K_Q) within a standard deviation of ± 0.1. The computer program PSEQUAD was utilized to compute conditional stability constants (log K_Q) which collected in Table 4.

It is noteworthy that normalized quenching curves plotted against the ligand-to-HSA ratios shown in Fig. 5 do not tend to zero, this can be explained by the partial quenching of Trp-214 fluorescence. This phenomenon was taken into consideration in our calculations (see details in our former work [23]). According to Fig. 5 and to the calculated log K_Q values in Table 4 the studied compounds show the different capability to quench the protein fluorescence. The emission intensity was practically unaltered in the case of **1b** and **2b**, consequently, no quenching constant could be computed; while remarkable binding of their
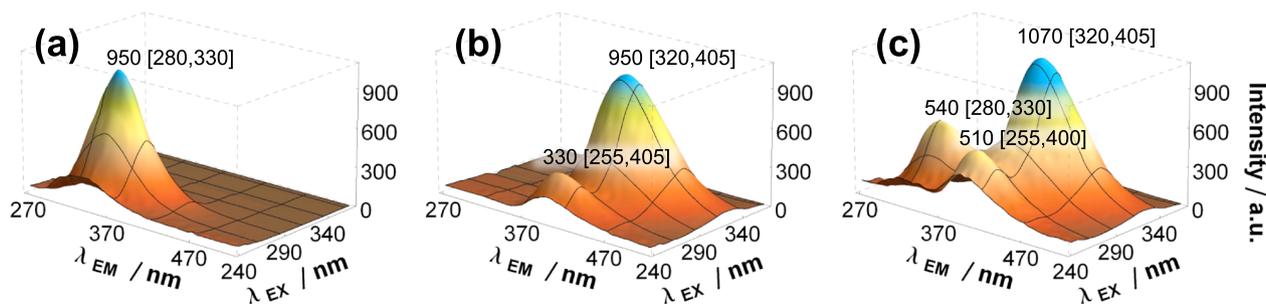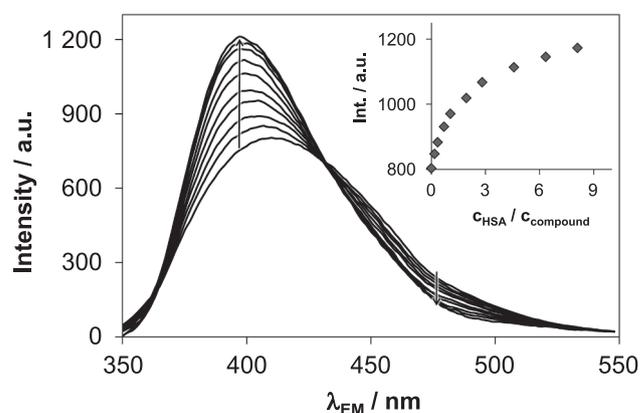
propyloxy analogs **1a** and **2a** were revealed at site 1 (subdomain IIA). The log K_Q values indicate a clear trend of the binding strength of the compounds at site 1 on HSA: **4a** > **4b** > **3a** ≥ **3b** > > **2a** > **1a**. Notably, the differences between the values obtained for **4a**, **4b**, **3a**, and **3b** is relatively small. According to the fluorescence quenching measurements most compounds (except **1b** and **2b**) bind in a great manner on site 1, and all propoxy derivatives show a somewhat higher affinity towards this site compared to their butoxy pairs. The determined binding constants (log $K_Q = 5.3$–6.0) are slightly higher on average compared to those of their close related analogs (log $K_Q = 4.8$–5.8) reported in our former work [23], but significantly lower than that of some reduced Schiff base coumarin compounds examined formerly by some of us [56].

As described in the former Section, the studied coumarin compounds are fluorescent themselves and the effect of albumin binding on their intrinsic fluorescence was also investigated. Three-dimensional fluorescence spectra recorded for **3a** and/or HSA (Fig. 6) clearly show that the peak of the compound is increased moderately upon binding to the protein while the peak belonging to the HSA is quenched. Fig. 7 shows the spectral and intensity changes of **3a** in the presence of increasing amount of HSA and an unequivocal increase in the intensity and slight blue shift of $\lambda_{(EM)}$ can be seen. Similar behavior was found for the compounds **4a**, **4b**, **1b**, and **2b** also, confirming the sensitivity of their intrinsic fluorescence to binding to HSA. However, the latter ones responded with a decrease in their intensity upon binding to the protein (see Fig. S6 and S7 in Supplementary Materials). Based on the changes of the emission intensity binding constants could be also computed. Calculated log K = 5.73 ± 0.1 for the **3a** – HSA system corresponds well to the value determined in the quenching experiment (log $K_Q = 5.75 \pm 0.1$), which strongly supports that Sudlow site 1 represents the only significant binding pocket for this compound.

Fig. 6. Three-dimensional fluorescence spectra of HSA (**a**) compound **3a** (**b**) and HSA – **3a** (1:11) system (**c**); peak intensities and wavelength coordinates (Intensity, [λ_{EX}, λ_{EM} expressed in nm]) are indicated in the figure ($c_{HSA} = 1\,\mu M$; $c_{comp} = 11\,\mu M$; $t = 25\,°C$; pH 7.40 (20 mM phosphate buffer); I = 0.10 M (KCl)).
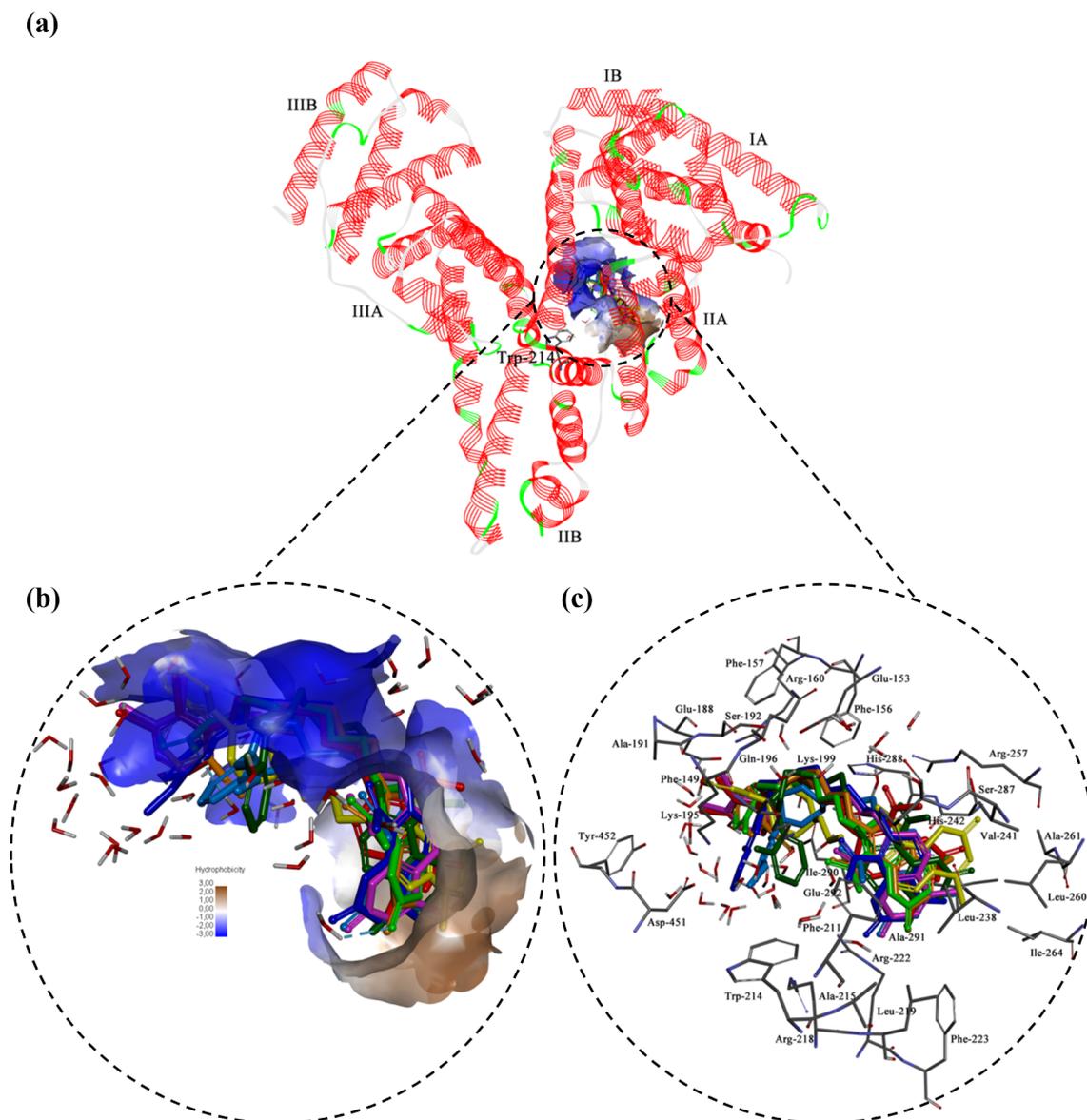
Fig. 8. View of coumarin derivatives in site 1 of HSA. (a) Structure of HSA showing the subdomains and binding sites of compounds **1a–4a** and **1b–4b**. Compounds around the binding pocket are shown as spheres. (b) The hydrophobic and hydrophilic amino acid residues surrounding the ligands. Surface hydrophobicity was depicted by the shaded colors: brown – the hydrophobic and blue – lipophilic regions. (c) Superposition of compounds: **1a** (green), **2a** (blue), **3a** (orange), **4a** (red), **1b** (dark green), **2b** (dark blue), **3b** (yellow) and **4b** (pink).

Noteworthy log K = 6.51 ± 0.1 and 6.23 ± 0.1 for **4a** and **4b** respectively are considerably higher than those of obtained in the quenching studies (log K_Q = 5.96 ± 0.1 and 5.88 ± 0.1). This finding refers to the existence of other binding sites of these two compounds on HSA besides site 1. Even **1b** and **2b** show moderate interaction with HSA (see Fig. S7 in Supplementary Materials) that takes place most probably not at site 1, since no Trp quenching could be detected for these ligands. Log K = 4.67 ± 0.1 could be computed for **2b** only.

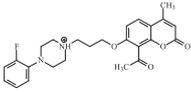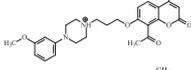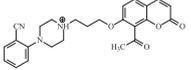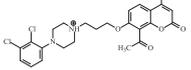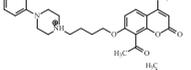### 3.4. Starting structures of the HSA – coumarins complexes by molecular docking
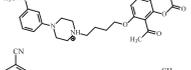
As mentioned previously, binding of ligands to HSA is extraordinarily eminent for the distribution and elimination of the drug as well as duration and intensity of its pharmacological or toxicological action. Molecular docking was conducted within subdomain IIA in Sudlow's site 1 formed by six helices (Fig. 8a) as the most probably pocket for 7-O-arylpiperazinyl-4-methylcoumarins. The most favorable

eight conformations of **1a–4a** and **1b–4b** with the lowest docking energy were found in 30 independent runs. The inner wall of the pocket of site 1 is formed by hydrophilic side chains (Glu-153, Ser-192, Lys-195, Lys-199, Arg-222, Arg-257, Ala-261, Ser-287, Ala-291, and Glu-292), and a hydrophobic region (formed by Phe-146, Phe-156, Phe-157, Trp-214, Leu-219, Leu-238, His-242, Leu-260, Ile-264, Ile-290, and Ala-291) (see Fig. 8b and 8c). As shown in Fig. 8c coumarins are on the entrance of the site 1 of HSA and the molecular distance between the coumarin ring and the core of the benzene ring in Trp-214 residues is in the range from 7.06 to 13.89 Å. The defined starting locations of tested coumarin derivatives in HSA pocket are similar. Molecular dynamics simulations were made to better simulate the interactions of **1a–4a** and **1b–4b** with the rests of amino acids or water molecules and to get binding free enthalpy of the hypothetical complexes.

3.5. Binding free enthalpy and interactions of tested coumarins with HSA

MD simulations were made for each HSA - ligand complex in

Table 5
Theoretical and experimental free enthalpy of binding to HSA, and average distance of ligand to tryptophan Trp-214 for coumarin derivatives.

Compound		ΔG_{bind} (kcal/mol)	ΔG_{exp}[a] (kcal/mol)	r (Å)
	1a	−7.69	−7.15	8.94
	2a	−7.84	−7.26	8.18
	3a	−8.64	−7.84	7.61
	4a	−9.66	−8.12	7.06
	1b	−6.36	–	13.89
	2b	−7.75	–	10.13
	3b	−8.45	−7.77	8.94
	4b	-8.89	−8.01	7.59

[a] ΔG_{exp} = -2.303 RT log K_Q

Sudlow site 1 as the pocket suggested for coumarin derivatives. The RMSD values between the ligand starting and the resulted average structures were low in all cases. The binding free enthalpy values for **1a**–**4a** and **1b**–**4b** calculated using the MM-PBSA method are presented in Table 5 together with the experimental values obtained using Gibbs' isotherm and log K_Q values (ΔG_{exp} = −2.303 RT log K_Q). The experimental values were not obtained for compounds **1b** and **2b** (see Section 3.3), suggesting that these two compounds interact with HSA beside site 1. The computational and experimental values of the free enthalpy differences are in the range of 0.54 to 1.54 kcalmol^{-1}. The resulting differences may be due by two reasons: one that the X-ray structure of the HSA from crystals even after MD simulation differs from that of the experimental aqueous conditions, and the second that the ligands do not interact effectively with the hypothetical pocket. The calculated strength of interactions with HSA decrease in the sequence: **4a** > **4b** > **3a** > **3b** > **2a** > **2b** > **1a** > **1b** (-9.66 kcalmol^{-1} > -8.89 kcalmol^{-1} > -8.64 kcalmol^{-1} > -8.45 kcalmol^{-1} > -7.84 kcalmol^{-1} > -7.75 kcalmol^{-1} > -7.69 kcalmol^{-1} > -6.36 kcalmol^{-1}, respectively). The MD resulting orientations of ligands are presented in Fig. 9 for compounds **1a**–**4a** with the propylene linker and in Fig. 10 for compounds **1b**–**4b** with the butylene linker. The coumarin rings of all tested compounds were similarly located within the hydrophobic binding pocket of HSA mainly surrounded by Leu-238, Leu-260, Ile-264, Ile-290, and Ala-291, whereas the acetyl group at 8-position makes hydrogen bonds primarily with Lys-199, and His-242, Arg-257, and Ser-287. The rest of the molecule elements (alkyl chains, piperazine and benzene rings) were the deciding factors showcasing the differences in binding modes with HSA. The propylene linker adopts an extended conformation in the complexes of compounds **1a**–**4a** with benzene ring twisted only in compound **2a**, while the butylene linker adopts a folded conformation in the complexes of compounds **1b**–**4b**.

From the experimental studies of HSA fluorescence quenching, it is clear that majority of tested compounds (except **1b** and **2b**) are located

next to the Trp-214 amino residue and show distinct differences in their binding ability. The MD simulation results showed that the location within the cavity of compounds **1a**, **2a** and **3a** is almost the same, and molecules are predominantly surrounded by interior pocket residues Glu-153, Ser-192, Lys-195, Lys-199, and Glu-292 creating electrostatic interactions and hydrogen bonds. Compound **3a** with the 2-cyanophenyl substituent is highly solvated by water molecules present inside the pocket of site 1, which can play an important role in binding of **3a** to HSA. The nearest distance of propoxy derivatives from Trp-214 residue is 7.06 Å for compound **4a** (Table 5), so the MD studies showed the probability of strong quenching caused by **4a** (Fig. 5a). The interaction between compound **4a** and HSA is dominated by hydrophobic contacts with Phe-149, Phe-156, Phe-157, Leu-238, Leu-260, Ile-290, and Ala-291, but there are also a number of specific electrostatic interactions and hydrogen bonds. Especially the carbonyl group of the acetyl substituent at 8-position forms hydrogen bonds with Arg-257, Ala-261 and Ser-267.

The butoxy derivatives **1b**–**4b** are located in site 1 in such a way that the distances to Trp-214 residue are 13.89 Å for compound **1b**, 10.13 Å for compound **2b**, 8.94 Å for compound **3b** and 7.59 Å for compound **4b**. These calculated distances stand in good agreement with the quenching efficacy (see Fig. 5) of the compounds. The long distance close to 14 Å can be an answer for the practically unaltered fluorescence intensity for **1b** and **2b** upon binding to HSA (see Fig. S5 in Supplementary Materials). Compounds **1b**, **2b** and **4b** are predicted to be accommodated in the HSA pocket in folded conformations, what is energetically unfavorable, and decreases the hydrophobic interactions with surrounding amino acids (Fig. 10). Compound **1b** forms the hydrogen bonds with Ser-192, Lys-199 and His-242 and creates electrostatic interaction with Lys-195 of HSA. The conformation of **3b** differs from conformations **1b**, **2b** and **4b** - the aromatic rings are located in opposed directions in relation to butyloxy linkers, and favorably interactions can be formed. Compound **3b** creates electrostatic and hydrogen bond interactions with interior pocket residues Glu-153, Glu-292, Lys-199 and Ala-291, and hydrophobic interactions with Ala-191.

4. Conclusions

To sum up, in this work we have evaluated eight 8-acetyl-7-*O*-arylpiperazinyl-4-methylcoumarin derivatives with strong binding ability towards 5-HT$_{1A}$ and 5-HT$_{2A}$ receptors aimed at gathering information about their potential application as orally administered antipsychotic agents. Theoretical values of drug likeness parameters as lipophilicity, topological polar surface area, and BBB permeation characteristics are in the regions for CNS drug candidates. The most promising compounds **4a** and **4b** have two Cl atoms at benzene ring. All compounds are partly protonated at pH 7.40, and their pK_a values are in the range 6.35–7.20. Studied coumarins can be metabolized by cytochrome P450 to aldehydes and hydroxy derivatives. Tested coumarins are predicted as P-glycoprotein inhibitors what can increase their rate of uptake by the BBB. Unfortunately, the tested 8-acetyl-7-*O*-arylpiperazinyl-4-methylcoumarin showed moderate-to-strong binding to human serum albumin. This phenomenon was studied experimentally and *in silico* in great detail. A logarithm of their experimental binding constants obtained from quenching measurements was in the range 5.25–5.96. Sudlow's site 1 was proposed as the significant binding pocket inside HSA for compounds **1a**, **2a**, **3a** and **3b**, while for compounds **1b** and **2b** the existence of other binding site is postulated, and for compounds **4a** and **4b**, the commitment of two binding sites of HSA. Theoretical analysis of complexes in Sudlow site 1 showed that hydrophobic interaction is less probably for compounds **1b** and **2b**, and their distance to Trp-214 is much longer than for other compounds. Theoretical and experimental results suggest that longer aliphatic linker between coumarin and piperazine moieties favored binding to HSA in other than Sudlow site 1 pocket. Overall the 8-acetyl-7-*O*-arylpiperazinyl-4-methylcoumarin derivatives represent valuable lead compounds to be

Fig. 9. Structures of the **1a** – HSA, **2a** – HSA, **3a** – HSA and **4a** – HSA complexes, and 2D view of all HSA residues interacting with the ligands resulting from MD simulations (residues involved in hydrogen bonding marked as green and cyan circles; in hydrophobic interactions marked as pink circle and electrostatic interactions marked as orange circle).
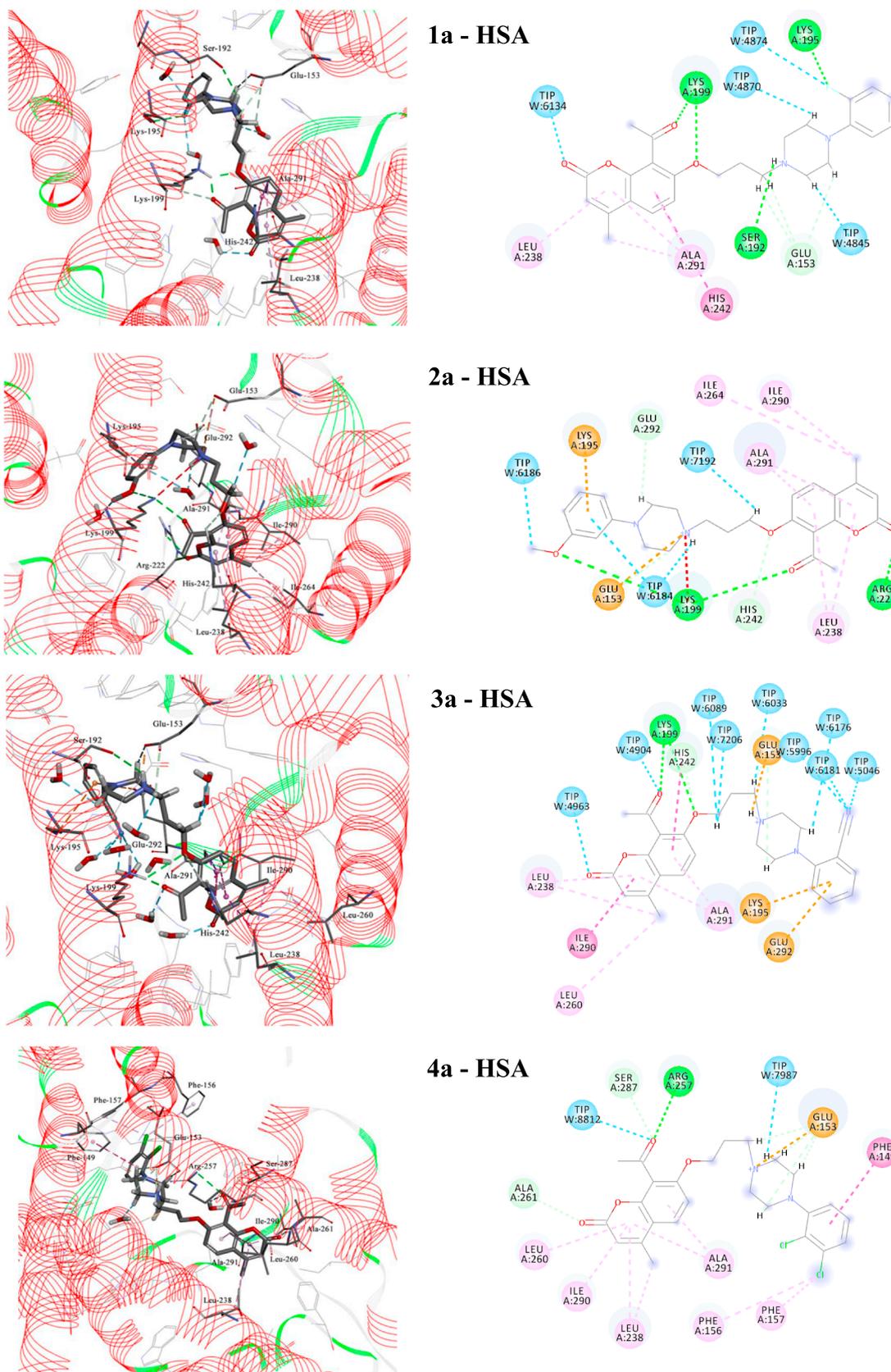
Fig. 10. Structures of the **1b** – HSA, **2b** – HSA, **3b** – HSA and **4b** – HSA complexes, and 2D view of all HSA residues interacting with the ligands resulting from MD simulations (residues involved in hydrogen bonding marked as green and cyan circles; in hydrophobic interactions marked as pink circle and electrostatic interactions marked as orange circle).
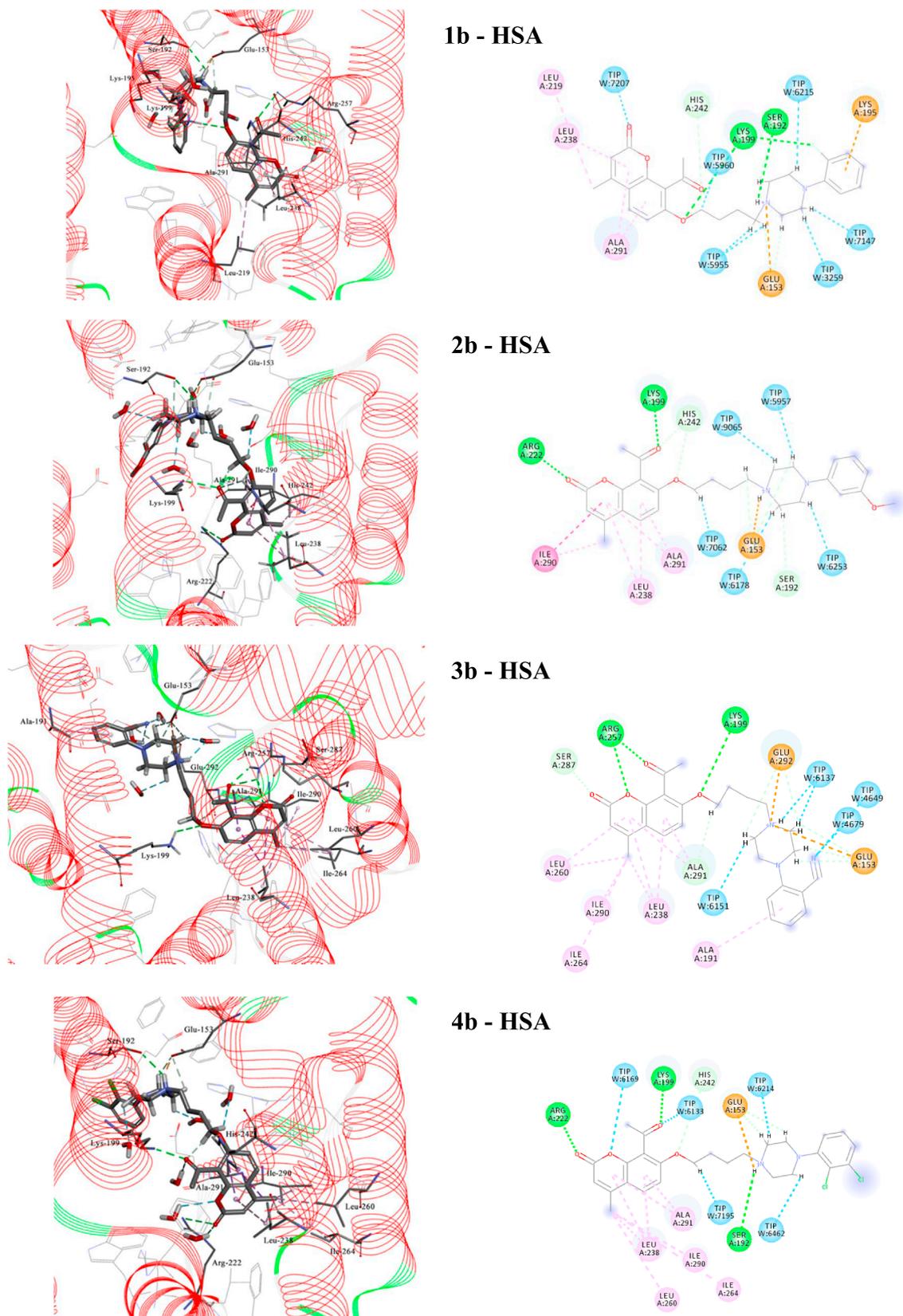
further studied in different preclinical assays as a possible treatment of diverse CNS diseases.

Conflict of interest

Acknowledgments

Appendix A. Supplementary material

Supplementary data to this article can be found online at https://doi.org/10.1016/j.bioorg.2018.11.034.

References

[1] P. Morgan, P.H. Van der Graaf, J. Arrowsmith, D.E. Feltner, K.S. Drummond, C.D. Wegner, S.D.A. Street, Can the flow of medicines be improved? Fundamental pharmacokinetic and pharmacological principles toward improving Phase II survival, Drug Discov. Today 17 (9–10) (2012) 419–424.

[2] W.M. Pardridge, Drug and gene targeting to the brain with molecular Trojan horses, Nat. Rev. Drug Discov. 1 (2) (2002) 131–139.

[3] E. Neuwelt, N.J. Abbott, L. Abrey, W.A. Banks, B. Blakley, T. Davis, B. Engelhardt, P. Grammas, M. Nedergaard, J. Nutt, W. Pardridge, G.A. Rosenberg, Q. Smith, L.R. Drewes, Strategies to advance translational research into brain barriers, Lancet Neurol. 7 (1) (2008) 84–96.

[4] G. Bazzoni, E. Dejana, Endothelial cell-to-cell junctions: molecular organization and role in vascular homeostasis, Physiol. Rev. 84 (3) (2004) 869–901.

[5] N.J. Abbott, A.A.K. Patabendige, D.E.M. Dolman, S.R. Yusof, D.J. Begley, Structure and function of the blood-brain barrier, Neurobiol. Dis. 37 (1) (2010) 13–25.

[6] W.A. Banks, Characteristics of compounds that cross the blood-brain barrier, BMC Neurol. 9 (Suppl 1) (2009) S3.

[7] M. Vastag, G.M. Keseru, Current in vitro and in silico models of blood-brain barrier penetration: a practical view, Curr. Opin. Drug Discov. Devel. 12 (1) (2009) 115–124.

[8] M.A. Musa, J.S. Cooperwood, M.O. Khan, A review of coumarin derivatives in pharmacotherapy of breast cancer, Curr. Med. Chem. 15 (26) (2008) 2664–2679.

[9] I. Kostova, Synthetic and natural coumarins as cytotoxic agents, Curr. Med. Chem. Anticancer Agents 5 (1) (2005) 29–46.

[10] T. Żołek, D. Maciejewska, Theoretical evaluation of ADMET properties for coumarin derivatives as compounds with therapeutic potential, Eur. J. Pharm. Sci. 109 (2017) 486–502.

[11] K. Skalicka-Wozniak, I.E. Orhan, G.A. Cordell, S.M. Nabavi, B. Budzynska, Implication of coumarins towards central nervous system disorders, Pharmacol. Res. 103 (2016) 188–203.

[12] Y. Chen, S. Wang, X. Xu, X. Liu, M. Yu, S. Zhao, S. Liu, Y. Qiu, T. Zhang, B.F. Liu, G. Zhang, Synthesis and biological investigation of coumarin piperazine (piperidine) derivatives as potential multireceptor atypical antipsychotics, J. Med. Chem. 56 (11) (2013) 4671–4690.

[13] J.C. Gonzalez-Gomez, L. Santana, E. Uriarte, J. Brea, M. Villazon, M.I. Loza, M. De Luca, M.E. Rivas, G.Y. Montenegro, J.A. Fontenla, New arylpiperazine derivatives with high affinity for alpha1A, D2 and 5-HT2A receptors, Bioorg. Med. Chem. Lett. 13 (2) (2003) 175–178.

[14] T. Kanazawa, Brain delivery of small interfering ribonucleic acid and drugs through intranasal administration with nano-sized polymer micelles, Med. Dev. (Auckl.) 8 (2015) 57–64.

[15] K.V. Sashidhara, A. Kumar, M. Kumar, S. Singh, M. Jain, M. Dikshit, Synthesis of novel 3-carboxamide-benzocoumarin derivatives as orally active antithrombotic agents, Bioorg. Med. Chem. Lett. 21 (23) (2011) 7034–7040.

[16] D.C. Carter, J.X. Ho, Structure of serum albumin, Adv. Prot. Chem. 45 (1994) 153–203.

[17] Y.Z. Zhang, B. Zhou, Y.X. Liu, C.X. Zhou, X.L. Ding, Y. Liu, Fluorescence study on the interaction of bovine serum albumin with p-aminoazobenzene, J. Fluoresc. 18 (1) (2008) 109–118.

[18] K. Yamasaki, V.T. Chuang, T. Maruyama, M. Otagiri, Albumin-drug interaction and its clinical implication, Biochim. Biophys. Acta 1830 (12) (2013) 5435–5443.

[19] Y.V. Il'ichev, J.L. Perry, J.D. Simon, Interaction of ochratoxin a with human serum albumin. Preferential binding of the dianion and pH effects, J. Phys. Chem. B 106 (2002) 452–459.

[20] K.J. Fehske, U. Schlafer, U. Wollert, W.E. Muller, Characterization of an important drug binding area on human serum albumin including the high-affinity binding sites of warfarin and azapropazone, Mol. Pharmacol. 21 (2) (1982) 387–393.

[21] I. Sjoholm, B. Ekman, A. Kober, I. Ljungstedt-Pahlman, B. Seiving, T. Sjodin,

[22] A.M. Zaton, J.M. Ferrer, J.C. Ruiz de Gordoa, M.A. Marquinez, Binding of coumarins to site I of human serum albumin. Effect of the fatty acids, Chem. Biol. Interact. 97 (2) (1995) 169–174.

[23] T. Żołek, E.A. Enyedy, K. Ostrowska, V. Posa, D. Maciejewska, Drug likeness prediction of 5-hydroxy-substituted coumarins with high affinity to 5-HT$_{1A}$ and 5-HT$_{2A}$ receptors, Eur. J. Pharm. Sci. (2018) 25–36.

[24] A.M.L. Zaton, J.P. Villamor, Study of heterocyle rings binding to human serum albumin, Chem.-Biol. Interact. 124 (1) (2000) 1–11.

[25] D. Li, B. Ji, H. Sun, Probing the binding of 8-Acetyl-7-hydroxycoumarin to human serum albumin by spectroscopic methods and molecular modeling, Spectrochim. Acta A Mol. Biomol. Spectrosc. 73 (1) (2009) 35–40.

[26] K. Ostrowska, K. Mlodzikowska, M. Gluch-Lutwin, A. Grybos, A. Siwek, Synthesis of a new series of aryl/heteroarylpiperazinyl derivatives of 8-acetyl-7-hydroxy-4-methylcoumarin with low nanomolar 5-HT$_{1A}$ affinities, Eur. J. Med. Chem. 137 (2017) 108–116.

[27] Dassault Systèmes BIOVIA, Discovery Studio Modeling Environment, Release 2017, Dassault Systèmes, San Diego, 2016.

[28] M.J. Frish, G.W. Trucks, H.B. Schlegel, G.E. Scuseria, M.A. Robb, J.R. Cheeseman, V.G. Zakrzewski, J.A.J. Montgomery, R.E. Stratmann, J.C. Burant, S. Dapprich, J.M. Millam, A.D. Daniels, K.N. Kudin, M.C. Strain, O. Farkas, J. Tomasi, V. Barone, M. Cossi, R. Cammi, B. Mennucci, C. Pomelli, C. Adamo, S. Clifford, J. Ochterski, G.A. Petersson, P.Y. Ayala, Q. Cui, K. Morokuma, D.K. Malick, A.D. Rabuck, K. Raghavachari, J.B. Foresman, J. Cioslowski, J.V. Ortiz, A.G. Baboul, B.B. Stefanov, G. Liu, A. Liashenko, P. Piskorz, I. Komaromi, R. Gomperts, R.L. Martin, D.J. Fox, T. Keith, M.A. Al-Laham, C.Y. Peng, A. Nanayakkara, C. Gonzalez, M.P. Challacombe, P.M.W. Gill, B. Johnson, W. Chen, M.W. Wong, J.L. Andres, C. Gonzalez, M. Head-Gordon, E.S. Replogle, J.A. Pople, Gaussian, Inc., Pittsburgh, PA, 2009.

[29] ADMET PredictorTM Simulations Plus, Inc., Lancaster, California, USA.

[30] G.M. Morris, R. Huey, W. Lindstrom, M.F. Sanner, R.K. Belew, D.S. Goodsell, A.J. Olson, AutoDock4 and AutoDockTools4: automated docking with selective receptor flexibility, J. Comput. Chem. 30 (2009) 2785–2791.

[31] B.R. Brooks, R.E. Bruccoleri, B.D. Olafson, D.J. States, S. Swaminathan, M. Karplus, Charmm – a program for macromolecular energy, minimization, and dynamics calculations, J. Comput. Chem. 4 (1983) 187–217.

[32] W.L. Jorgensen, J. Chandrasekhar, J.D. Madura, R.W. Impey, M.L. Klein, Comparison of simple potential functions for simulating liquid water, J. Chem. Phys. 79 (1983) 926–935.

[33] L. Verlet, Computer experiments on classical fluids. I. Thermodynamical properties of Lennard-Jones molecules, Phys. Rev. 159 (1967) 98–103.

[34] P.A. Kollman, I. Massova, C. Reyes, B. Kuhn, S. Huo, L. Chong, M. Lee, T. Lee, Y. Duan, W. Wang, O. Donini, P. Cieplak, J. Srinivasan, D.A. Case, T.E. Cheatham, Calculating structures and free energies of complex molecules: combining molecular mechanics and continuum models, Acc Chem. Res. 33 (2000) 889–897.

[35] G.H. Beaven, S.H. Chen, A. d' Albis, W.B. Gratzer, A spectroscopic study of the haemin–human-serum-albumin system, Eur. J. Biochem. 41 (3) (1974) 539–546.

[36] L. Zékány, I. Nagypál, D.J.E. Leggett, Computational Methods for the Determination of Formation Constants, Plenum Press, New York, 1985, pp. 291–353.

[37] O. Domotor, C.G. Hartinger, A.K. Bytzek, T. Kiss, B.K. Keppler, E.A. Enyedy, Characterization of the binding sites of the anticancer ruthenium(III) complexes KP1019 and KP1339 on human serum albumin via competition studies, J. Biol. Inorg. Chem. 18 (1) (2013) 9–17.

[38] T. Sakaeda, N. Okamura, S. Nagata, T. Yagami, M. Horinouchi, K. Okumura, F. Yamashita, M. Hashida, Molecular and pharmacokinetic properties of 222 commercially available oral drugs in humans, Biol. Pharm. Bull. 24 (8) (2001) 935–940.

[39] M.H. Abraham, F. Martins, R.C. Mitchell, C.J. Salter, Hydrogen bonding. 47. Characterization of the ethylene glycol-heptane partition system: hydrogen bond acidity and basicity of peptides, J. Pharm. Sci. 88 (2) (1999) 241–247.

[40] T.T. Wager, R.Y. Chandrasekaran, X. Hou, M.D. Troutman, P.R. Verhoest, A. Villalobos, Y. Will, Defining desirable central nervous system drug space through the alignment of molecular properties, in vitro ADME, and safety attributes, ACS Chem. Neurosci. 1 (6) (2010) 420–434.

[41] N.A. Meanwell, Improving drug candidates by design: a focus on physicochemical properties as a means of improving compound disposition and safety, Chem. Res. Toxicol. 24 (9) (2011) 1420–1456.

[42] J. Kelder, P.D. Grootenhuis, D.M. Bayada, L.P. Delbressine, J.P. Ploemen, Polar molecular surface as a dominating determinant for oral absorption and brain penetration of drugs, Pharm. Res. 16 (10) (1999) 1514–1519.

[43] H. van de Waterbeemd, G. Camenisch, G. Folkers, J.R. Chretien, O.A. Raevsky, Estimation of blood-brain barrier crossing of drugs using molecular size and shape, and H-bonding descriptors, J. Drug Target. 6 (2) (1998) 151–165.

[44] W.M. Pardridge, Drug transport across the blood-brain barrier, J. Cereb. Blood Flow Metab. 32 (11) (2012) 1959–1972.

[45] T.B. Fernandes, M.C.F. Segretti, M.C. Polli, R. Parise, Analysis of the applicability and use of Lipinski's Rule for Central Nervous System Drugs, Lett. Drug Des. Discov. 13 (10) (2016) 999–1006.

[46] S.A. Hitchcock, Blood-brain barrier permeability considerations for CNS-targeted compound library design, Curr. Opin. Chem. Biol. 12 (3) (2008) 318–323.

[47] H. Pajouhesh, G.R. Lenz, Medicinal chemical properties of successful central nervous system drugs, NeuroRx 2 (4) (2005) 541–553.

[48] H. Fischer, R. Gottschlich, A. Seelig, Blood-brain barrier permeation: molecular parameters governing passive diffusion, J. Membr. Biol. 165 (3) (1998) 201–211.

[49] T.J. Raub, B.S. Lutzke, P.K. Andrus, G.A. Sawada, B.A. Staton, Early preclinical evaluation of brain exposure in support of hit identification and lead optimization,

Binding of drugs to human serum albumin:XI. The specificity of three binding sites as studied with albumin immobilized in microparticles, Mol. Pharmacol. 16 (3) (1979) 767–777.

Biotechnol. Pharm. Asp 4 (2006) 355.

[50] J. Weiss, S.M. Dormann, M. Martin-Facklam, C.J. Kerpen, N. Ketabi-Kiyanvash, W.E. Haefeli, Inhibition of P-glycoprotein by newer antidepressants, J. Pharmacol. Exp. Ther. 305 (1) (2003) 197–204.

[51] F.E. O'Brien, G.M. Moloney, K.A. Scott, R.M. O'Connor, G. Clarke, T.G. Dinan, B.T. Griffin, J.F. Cryan, Chronic P-glycoprotein inhibition increases the brain concentration of escitalopram: potential implications for treating depression, Pharmacol. Res. Perspect. 3 (6) (2015) e00190.

[52] B.N. Matto, Absorption and fluorescence spectra of coumarins, Trans. Faraday Soc. 52 (1956) 1184–1194.

[53] T.J. Peters, All About Albumin, Biochemistry, Genetics, and Medical Applications,

Academic Press, New York, 1996.

[54] G. Fanali, A. di Masi, V. Trezza, M. Marino, M. Fasano, P. Ascenzi, Human serum albumin: from bench to bedside, Mol. Aspects Med. 33 (3) (2012) 209–290.

[55] G. Sudlow, D.J. Birkett, D.N. Wade, Further characterization of specific drug binding sites on human serum albumin, Mol. Pharmacol. 12 (6) (1976) 1052–1061.

[56] O. Domotor, T. Tuccinardi, D. Karcz, M. Walsh, B.S. Creaven, E.A. Enyedy, Interaction of anticancer reduced Schiff base coumarin derivatives with human serum albumin investigated by fluorescence quenching and molecular modeling, Bioorg. Chem. 52 (2014) 16–23.

[57] X.L. Ma, C. Chen, J. Yang, Predictive model of blood-brain barrier penetration of organic compounds, Acta Pharmacol. Sin. 26 (4) (2005) 500–512.